



# Measurement of surface-checking in sliced lamellae-based engineered wood flooring using digital image correlation

Victor Grubii<sup>1</sup> · Jimmy Johansson<sup>1</sup> · Ola Dagbro<sup>1</sup>

Received: 17 November 2022 / Accepted: 27 July 2023 / Published online: 14 August 2023  
© The Author(s) 2023

## Abstract

The lack of quantitative methods for surface-checking measurements may hinder improving the product characteristics of engineered wood flooring products built with sliced top-layer lamellae. This study evaluated the digital image correlation method for its applicability to surface checking measurements in engineered wood flooring elements with the top-layer comprising the plain sliced lamellae of oak (*Quercus* spp.) species with nominal thicknesses of 1.5–4.5 mm. The method involves observing full-field surface displacements of the sliced lamellae-based wood flooring specimens subjected to an accelerated sorption/desorption cycle. Detection of surface checks relates to discontinuities in surface displacements which can be interpreted from the output strain data as strain peak regions. Additionally, a surface-checking index was defined to describe the extension of surface-checking. Exposure tests were performed on a combination of coating presence and a different number of testing cycles. The main findings provide insight into the method procedure parameters, such as exposure duration, climate conditions, analysis parameters and recommendations regarding the digital image correlation setup settings and specimen manufacturing.

## 1 Introduction

Currently, the main product category of engineered wood flooring (EWF) is represented by solid wood-based multi-layered parquet elements with an approximate production of 74 mln. m<sup>2</sup> in Europe alone (FEP 2021). Raw material availability and production and product costs represent the main drivers for the relatively low share of wood (below 5%) as a covering material (Jonsson 2005; FEP 2021). One way to improve the material yield in the final products and increase the sustainability of EWF elements may be to use a slicing technique for top-layer production instead of sawing. For instance, valuable wood material waste while sawing the thin lamellae for EWF top-layer production is estimated to be about 20–30% of the timber volume. Additionally, sawdust-free processing would benefit a production unit's fire

and health safety. Some drawbacks of wood slicing are the need for more complex logistics, higher production costs and investment needs compared to common sawmills.

A significant disadvantage of sliced wood compared to sawn wood is the material quality issues. During slicing, the wood is fractured ahead of the cutting tool, with the resultant slicing checks defect. Slicing checks reduce veneer and sliced lamellae (SL) strength perpendicular to the grain (Pfriem and Buchelt 2011), which is presumably impacting surface cracks or checking of the finished engineered wood products (EWP). A *check*, or a *crack*, can be defined as the morphological separation or opening of wood along the grain. *Surface-checking* (SC) can be defined as the sum of checks and cracks over a surface area extending to the top surface. Veneer-based EWP develop surface checks due to the propagation of slicing checks and the fracture of the coating layer when subjected to drying conditions (Cassens et al. 2003; Leavengood et al. 2011; Burnard et al. 2018). This phenomenon occurs mostly during a product's in-service life, reducing customer value or resulting in high claim or repair costs. In addition, SL's low toughness imposes challenges during production, as standard material handling results in poor product throughput due to quality issues such as edge-tearing (Grubii and Johansson 2019). Consequently,

✉ Victor Grubii  
victor.grubii@lnu.se

Jimmy Johansson  
jimmy.johansson@lnu.se

Ola Dagbro  
ola.dagbro@lnu.se

<sup>1</sup> Department of Forestry and Wood Technology, Linnaeus University, SE 351-95 Växjö, Sweden

SC defect can be considered a limiting factor in using SL for several EWP, including EWF elements.

To better understand the SC defect and improve the quality of SL-based EWPs, adequate methods for SC detection must be available. SC measurement methods most commonly rely on visual inspection (Cassens et al. 2003; DeValance et al. 2007; Leavengood et al. 2011). However, this method requires extensive resources for evaluation and has a limited output on the SC information. Another significant disadvantage of the visual inspection method is the need for a physical check opening at the moment of inspection and the associated time cost. Inspection time reduction and fidelity maximisation are the main requirements for incorporating quantitative methods in SL-based EWP product development.

In a proof-of-concept study, Kang et al. (2006, 2011) showed that with the help of digital image correlation (DIC), checks in solid wood can be observed in situ early during a drying step as the zones of strain peak. Similarly, Mallet et al. (2018) used DIC to observe surface cracks in outdoor solid wood decking elements. Burnard et al. (2018) used DIC inspection and developed a segmentation procedure for SC detection in plywood face veneers based on the signature strain peak threshold. They proposed a surface quality parameter, check density, which was determined by summing the segmented check area based on a strain threshold of 2.5%.

The DIC method's main advantages compared with traditional image-vision methods for SC detection in wood consist in reduced inspection time, that is, less need for physical checking and higher fidelity. These factors influenced the DIC method selection for studying SC in SL-based EWF elements. Some disadvantages of the DIC method are the need for a particular sample preparation by applying a specific speckle pattern, computation costs and DIC output dependency on selected DIC parameters (computational method, window size, noise penalty rate etc.).

Unlike the materials previously studied with the DIC technique, the SL-based EWF element structure is somewhat unique, that is a thick top-layer lamella, predominantly of oak (*Quercus* spp.) species, pressed onto a solid wood core and a thin back-end layer of softwood rotary-cut veneer. These aspects of the EWF structure may impose challenges when studied with the 2D–DIC methodology, for example, dimensional stability, check opening duration and extent. Therefore, studying the DIC method's suitability for EWF SC measurement is highly important.

The main objectives of this study were to evaluate the DIC parameters, procedures and testing setup requirements regarding particularities of EWF specimens. Significant outcomes of this study include the use of DIC output for check segmentation and analysis procedures. The specific objectives of the current study were to propose a SC parameter,

discuss the limitations of the DIC method for the intended SC detection application, and suggest further optimisation needs.

## 2 Materials and methods

The method used in this study involved inducing a steep drying gradient in SL-based EWF specimens and observing surface displacements using a 2D–DIC method. The DIC algorithm interprets surface discontinuities related to SC as regions of strain peaks. The full-field strain maps were then processed to determine actual check morphological properties.

### 2.1 Specimen preparation

EWF specimens that were part of this study were manually produced in a carpentry workshop. The EWF top-layers were oak (*Quercus robur* L. and *Quercus petraea* (Matt.) Liebl.) SL, produced using plain (vertical) slicing from freshly sawn slabs. The nominal thicknesses of the studied SL were 1.5, 2.5, 3.5, and 4.5 mm, chosen as possible top-layer lamellae thicknesses for EWF elements.

An EWF specimen structure and material positioning are illustrated schematically in Fig. 1. The SL were selected from the middle part of the cut slab, where the least variation in thickness was expected. The cores used to manufacture EWF elements were supplied by a local flooring manufacturer and represented standard solid wood softwood lamellae

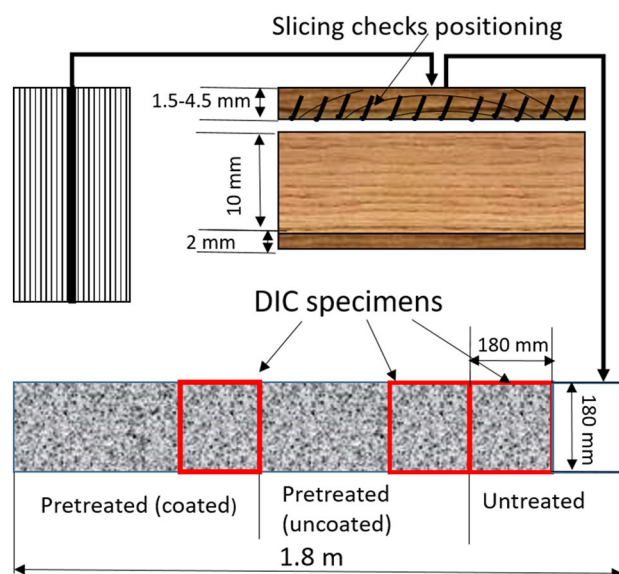


**Fig. 1** Schematic representation of specimen structure and material positioning of this study; SL position within slicing block (upper-left), structure of the EWF elements (upper-right) and position of the DIC specimens within the EWF element

glued perpendicularly onto a rotary-cut softwood veneer back-end layer. Both the cores and SL were conditioned at 21 °C and 40% RH for 2 weeks and 1 week, respectively.

The EWF elements were pressed at 90 °C for 5–10 min, depending on the top layer thickness, while the applied pressure was 6 MPa/m<sup>2</sup>, as recommended by the adhesive manufacturer. A two-component UF adhesive was manually spread at 170 g/m<sup>2</sup>. Full-length EWF elements were initially coated using a standard indoor lacquer system via a conveyor spray machine. In a series of pre-tests, no check or signature strain peaks were detected on the coated EWF specimens. The lack of detectable surface strain peak patterns could be explained by various factors, such as (1) the moisture “sealing” effect of the lacquer layer; (2) short-duration dry climate exposure; or (3) a mild drying gradient defined by a wet and dry condition consisting of 80% RH 20 °C and 20% RH 20 °C, respectively. Consequently, the remaining parts of the initial EWF elements were re-sanded to remove the coating layer, and the cumulative sanding thickness was 1 mm from the top and tight side of the SL. Subsequently, the EWF elements were stored at a climate of 21 °C and 65% RH for 1 week before specimen manufacturing. The specimens used in this study were produced from both coated and uncoated parts of the EWF elements.

The selected specimens for the DIC procedure testing were grouped into three categories: coated specimens exposed to two sorption/desorption cycles, uncoated specimens exposed to two sorption/desorption cycles and uncoated specimens exposed to one sorption/desorption cycle (Fig. 1). The number of sorption/desorption cycles was evaluated to strongly impact the characteristics of SC. Therefore, the first two categories were combined into a *pre-treated* group, and the last remained *untreated*. The resulting number of specimens per group and independent variable, SL thickness, is shown in Table 1. The DIC pattern was applied using an airbrush, which allowed for speckle homogeneity. First, a thin layer of white paint was applied to the entire surface of the EWF element. After approximately 48 h, black paint speckles were sprayed on the surface of the EWF elements, and the DIC pattern was controlled by

adjusting the nozzle opening and distance of spraying. The substance used for white and black speckles was a water-based paint for indoor wood applications, chosen with the assumption of an effect similar to possible EWF finishes. Before the DIC procedure began, the specimens were edge-coated with a thin silicone layer and wrapped in plastic foil on the edges and back surfaces.

## 2.2 Testing procedures

### 2.2.1 DIC testing procedures

The DIC procedure began with exposing the EWF specimens to a humid but realistic indoor climate. The humid exposure climate consisted of 85% RH and 21 °C for at least 48 h, achieved using a standard laboratory 1 m<sup>3</sup> climate chamber. The specimens were quickly glued to a polycarbonate plate using hot-melt glue between the humid–dry climate exposures to limit out-of-plane movement due to shrinking. Afterwards, the specimens were placed into the DIC acquisition climate chamber at 30 °C and 20% RH. Due to the opening of the climate chamber's door, the RH initially increased to about 25–30% RH and gradually reduced after ca. 30 min to the set value.

The DIC experimental setup consisted of a fixed camera placed over a specimen holder. Image acquisition was performed using a DMK 33GX183 camera with a Fujinon CF25ZA-1S 23MP 25 mm focal length lens at f/1.8. The illumination source was a single-ring SVL R80 light. The working distance was 1.11 m. With this setup, six specimens with nominal dimensions of 180 × 180 mm were recorded simultaneously. The resulting resolution of the digital images was 8.9 pixels/mm (Fig. 2). Image acquisition was performed at one-hour intervals for a total acquisition period of 48 h.

### 2.2.2 DIC algorithm

The DIC analysis was performed using the augmented Lagrangian digital image correlation (ALDIC) MATLAB algorithm (Yang and Bhattacharya 2019; Yang 2020). The advantage of the given algorithm is a combination of local and global subset displacement convergence, resulting in good compatibility and a low time cost. Displacements and strain were computed using the finite difference method for an infinitesimal strain type. The algorithm incorporated image enhancement by normalisation to limit the correspondence issue of the DIC method.

A DIC optical system bias can be validated by evaluating a non-deformed object of interest through multiple frames. Accuracy is represented by the variation in mean observation, and precision is a measure of standard error (Burnard et al. 2018). Five images were recorded at two-second

**Table 1** Specimen number and characteristics part of this study

Thickness [mm]	No. of specimens		
	Pretreated		Untreated uncoated
	Coated	Uncoated	
1.5	2	1	1
2.5	2	1	2
3.5	3	1	2
4.5	0	1	2
Total	7	4	7

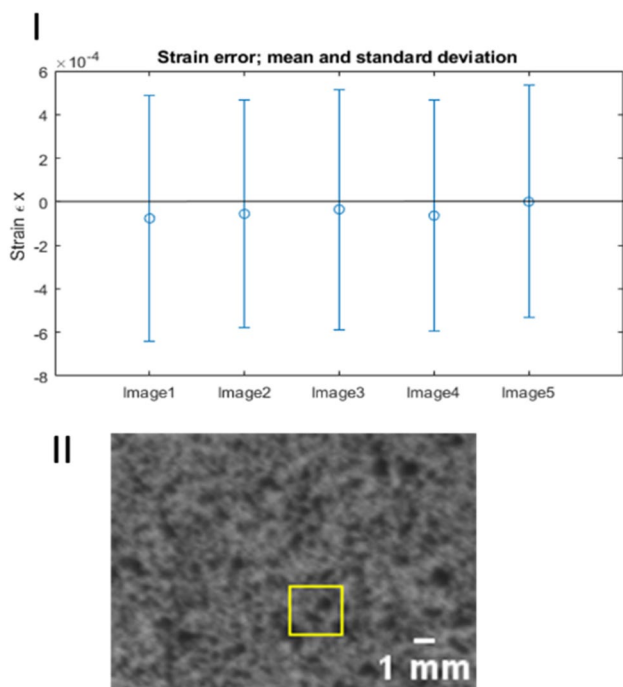


**Fig. 2** Strain error measured on the optical system used for the 2D-DIC study. Points represent mean value and error bars represent the standard deviation (I); raw DIC pattern and relative size of a subset (II)

intervals at the testing setup, assuming no displacements occurred. After that, displacements and strains across the grain were measured using the DIC algorithm. The accuracy error of the optical system was determined to be 0.67%, and the precision error was 3.67% of the strain threshold rate (Fig. 2).

The output of the DIC is strongly dependent on the subset size and subset step parameters. An optimal speckle size is recommended to vary between 3 to 5 pixels and determines a minimum subset size of  $15 \times 15$  pixels<sup>2</sup> with practical recommendations for larger subset sizes if pattern size and density are not constant over the region of interest (International Digital Image Correlation Society et al. 2018). The subset step size is typically one-third to one-half of the subset size. However, a lower step size may be required to capture small features close to the subset edges (International Digital Image Correlation Society et al. 2018). To determine the appropriate subset size and step, a series of low-incremental DIC analyses by varying the subset size from 10 to 50 pixels and step size from 2 to 15 pixels were performed on testing specimens. The optimal DIC post-processing settings were selected based on a few criteria. The first selection criterion was algorithm convergence, as a higher subset size to step ratio increased the incidence of non-converged points above the 0.1% non-convergence penalty. The second selection criterion was a weighting of the following aspects: the

amount of noise and random error, validation with manually observed checks, a desired high spatial resolution to detect narrow-spaced checks, a relevant strain threshold rate to detect the entire size spectrum of SC as early as possible during the dry climate exposure and computational time. After considering these criteria, a subset size of 20 pixels and a subset step of 5 pixels was identified as suitable for the specimen analysis. Lowering DIC parameters values resulted in high noise and impractically high computation costs. Furthermore, in agreement with general knowledge, a random error could be observed at approximately 14 pixels and a smaller subset size.

### 2.2.3 SC analysis

Checks can be detected due to surface displacement discontinuities in the surface body when a check occurs. This aspect is interpreted by the DIC algorithm into regions of strain peaks when compared to the unchecked area. Subsequently, strain maps need to be transformed to extract the positions of the checks relative to a specific strain threshold. The check position can be obtained by segmentation using a global strain threshold value, as in Burnard et al. (2018). The strain threshold in the case of the tested EWF specimens was 1.5% and was established based on the smallest observed checks.

After the segmentation step, the inspected areas may contain noise. A morphological filter was applied to reduce the regions detected with a physical length below 2 mm and a length-to-width ratio below two. This type of noise was primarily due to the DIC pattern artefacts and, more rarely, due to discontinuities in the segmented checks. Due to the reduced size of the removed particles, this step is believed not to influence the results significantly.

A variable that expresses the quality of a veneered surface regarding SC and DIC output capability was defined as a Checking Index (CI). The CI was determined regarding the total length of checks ( $C_L$  in m) over an inspected area ( $A$  in m<sup>2</sup>, in Eq. 1).

$$CI = \frac{\sum C_L}{A} \quad [\text{m/m}^2] \quad (1)$$

### 2.2.4 Method validation

Method validation was performed to evaluate measurement bias. For this purpose, CI was calculated by manually measuring SC using a transmitted-light microscope. Additionally, eighty true positive checks from the eight most-checked specimens were selected to evaluate measurement bias at the check level. Measurement and method's fixed and proportional bias were calculated using model II simple linear

regression analysis using the lmodel2 R package. The high data correlation and same variables units indicate the possible use of major axis (MA) regression (Ludbrook 2010) or ranged major axis (RMA) in the case of differences in error variances between axes (heteroscedasticity) (Legendre and Legendre 1998).

### 3 Results and discussion

#### 3.1 Method validation

The SC of SL-based EWF specimens was correlated with the development of strain peaks when monitored using a DIC inspection. The extent and period of SC depended on material and testing conditions. An example of the developing surface strains and check segmentation output is presented in Fig. 3. Small checks, i.e. thin checks that are visible under a close-up inspection or observation under a magnified glass, were observed to correspond to low strain, for example, 1.5–2.5%, even after prolonged exposure. Correspondingly, the global strain threshold value of 1.5% was considered to detect the lowest visible checks. Differently, wide checks typically correspond to a strain rate equal to and higher than 3%.

The results of MA and RMA regression analysis (Table 2) indicate the existence of fixed and proportionate bias for individual check measurement. Fixed bias is present when intercepts' 95% confidence interval does not include zero, and proportionate bias is when the slope's 95% confidence interval does not include one. Fixed bias refers to the detection method outputting constant higher or lower values. Higher detected vs. measured check length measurements were probably due to the DIC particularity of strain averaging over the measuring window and the check-bridging effect between two closely spaced check tips. A lower check length detection was probably due to a possible check extension after the acquisition phase ended, but also, low deformations in certain check's middle areas resulted in the output of fragmented checks. The proportional bias relates to significant error variance for short checks, e.g. up to 20 mm in length, probably due to strain averaging over measuring window and check fragmentation.

Measured vs. detected CI regression results indicate a lack of fixed bias, hence the existence of proportionate bias. Proportionate bias is thought to originate from residual increase for an increase in detected CI. The reason for that could be the detection of various surface deformations, such as cracks around knots and sub-surface slicing checks. The correlation  $r$  (Pearson's  $r$ ) coefficient between detected and measured CI was calculated to be 0.984, indicating a good fit between measured and detected values (Fig. 4).

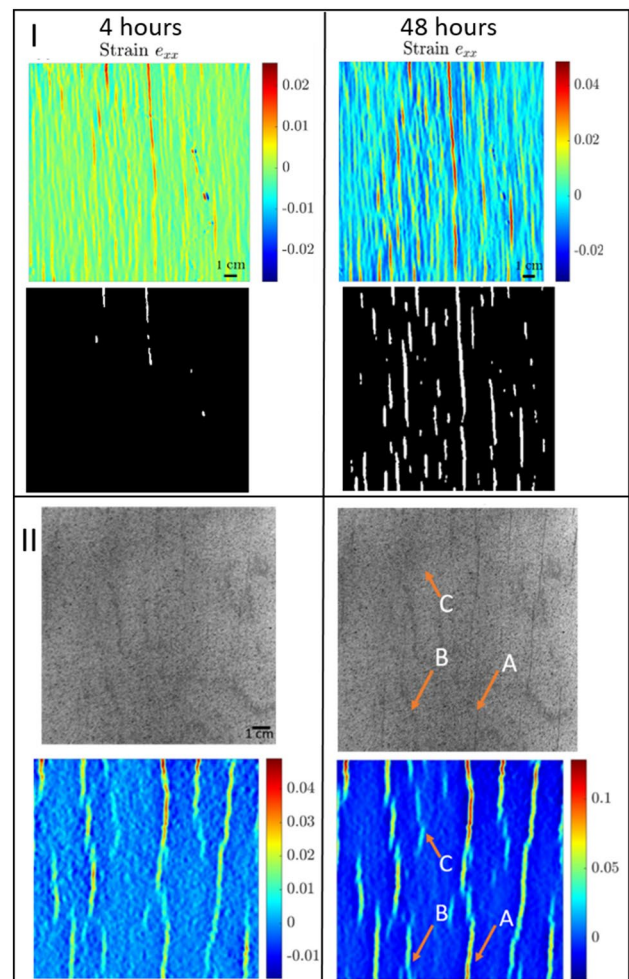


**Fig. 3** Example of strain peaks development after 4 and 48 h of exposure to a dry climate for an untreated and uncoated specimen and resulting checking measurement (I) and a coated and pretreated specimen (II) with corresponding DIC pattern surface, example of A—large, B—medium and C—smallest visible check

#### 3.2 Surface-checking

Strain peak intensity and CI were recorded to increase during the total inspection time. To capture this, Fig. 5 shows the mean strain development relevant to check formation observed for both untreated and pretreated specimens. The data were extracted based on strain above 2.5% for the last frame of the 48 h of exposure time. It can be observed that specimens containing checks due to the pretreatment developed strain peaks faster than the untreated specimens. The reason for that is thought to be due to reduced surface strength and area when checks propagate to the surface. For untreated specimens, a minimum of nine hours were required to reach the minimum considered strain rate equivalent to small checks (1.5%) and about 24 h to reach a strain rate equivalent to visible checks (2.5%).

**Table 2** Mode II regression results for individual check length (\*) and CI (\*\*) measurements

n* = 80			r* = 0.989	r-square* = 0.979	Number permutations*, ** = 99
n** = 18			r** = 0.984	r-square** = 0.968	
	Intercept	Slope	Angle(degrees)		P-permutation
MA*	-1.210	1.048	46.347		0.01
RMA*	-1.213	1.048	46.349		0.01
MA**	-2.250	1.271	51.808		0.01
RMA**	-2.082	1.263	51.646		0.01
	95% C.I. Intercept		95% C.I. Slope		
	Lower bound	Upper bound	Lower bound	Upper bound	
MA*	-2.383	-0.078	1.011	1.080	
RMA*	-2.386	-0.080	1.013	1.084	
MA**	-5.195	0.367	1.156	1.399	
RMA**	-4.956	0.565	1.148	1.389	

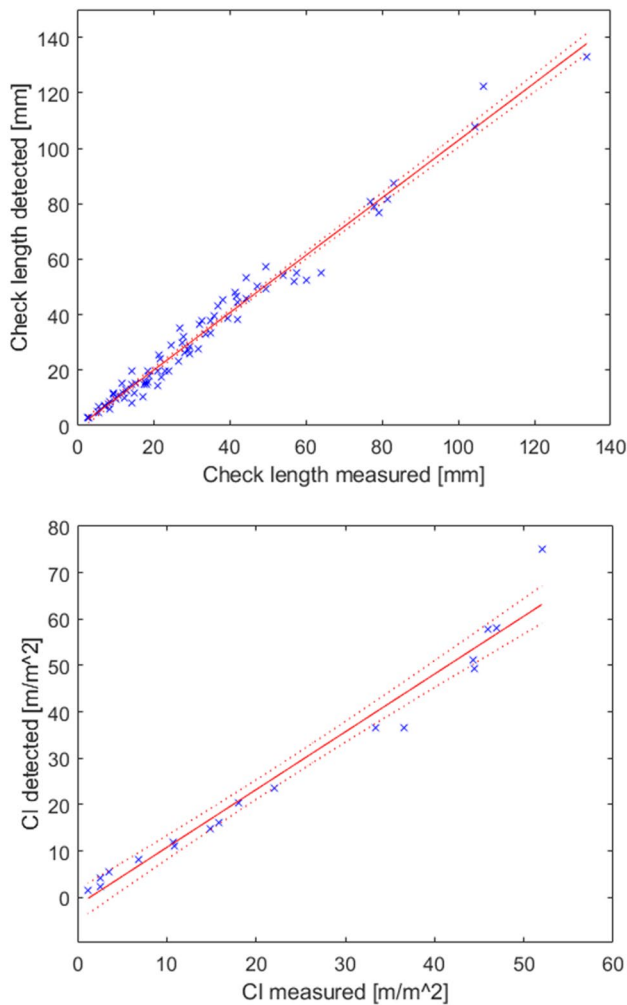


**Fig. 4** Measured vs. detected values and regression fit for check length (upper) and CI (lower)

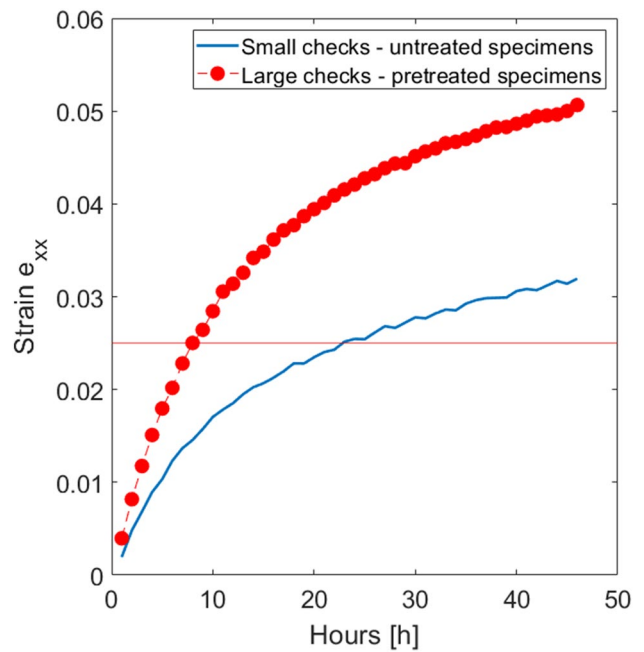


**Fig. 5** Mean results for strain intensity development corresponding to strain peak areas ( $\epsilon \geq 0.025$ ) detected at the end of the dry climate exposure for specimens with low checking (untreated specimens) and specimens containing extensive checking (pretreated specimens)

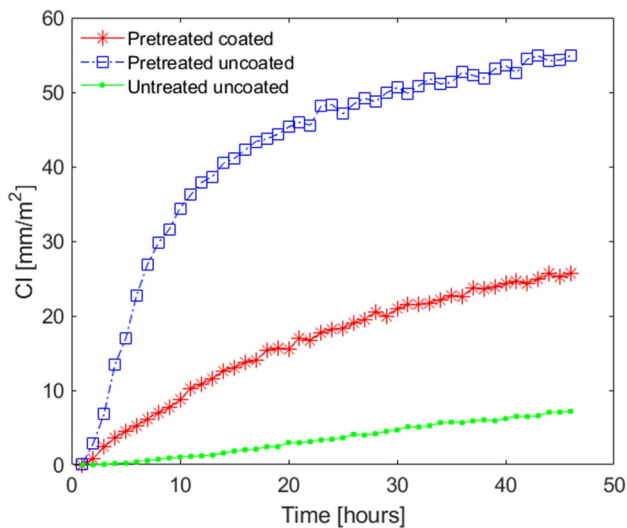
The results of SC based on the highest measured CI values are shown in Table 3. The most checking was detected on pretreated specimens that lacked surface coating for 1.5 mm—thick SL. A higher CI for uncoated specimens (average 55.2 mm/m<sup>2</sup>) vs. coated specimens (average 26.1 mm/m<sup>2</sup>) can be explained by the moisture-barrier effect of the coating layer on the drying gradient. The least checking was observed for the uncoated and untreated specimens (average 10.8 m/m<sup>2</sup>). In this case, CI grew slowly over the

**Table 3** CI results based on specimen thickness and category

Thickness [mm]	CI [m/m <sup>2</sup> ]		
	Pretreated		Untreated
	Coated	Uncoated	
1.5	47.22*	75.17	11.00
2.5	12.85*	51.59	9.64*
3.5	20.91**	36.46	19.45*
4.5	Not available	58.21	14.91*

\*Average for two specimens

\*\*Average for three specimens

**Fig. 6** Mean CI over the time of exposure in EWF specimens in relation to coating and exposure cycles (pretreated/untreated specimens)

exposure time, with the highest increase between 15 and 35 h of exposure (Fig. 6). The tendency for curve flattening of the CI could be observed at approximately 42–43 h during dry climate exposure. Coated and unchecked specimens (i.e., real-life products) would probably inherit a CI peak later than that tested in this study and are subject to further investigation. The exact quantification and prediction of all surface checks of an SL-based EWF are impossible, as smaller checks emerge continuously during drying. This highlights another potential limitation of the DIC method, namely, that a clear displacement gradient around the check must be present during the acquisition. Hence, measurement of SC in the early stages during drying may indicate long-term SC behaviour (Burnard et al. 2018).

### 3.3 DIC parameters

DIC parameters, such as subset size and step, directly influence the results and performance of the investigation, for

example, its convergence and accuracy. The DIC parameters must be decided based on a trade-off between spatial resolution and the limitation of the random strain error. Image acquisition settings and speckle pattern characteristics limit spatial resolution.

The effect of the subset size on the measured strain rate is shown in Fig. 7. Measured strain decreased with an increase in the subset size. It can also be observed that a high subset size would average the strain over a greater area, lowering the risk of strain error. The drawback of high subset size is the low spatial resolution or precision of strain measurements. In the case of check segmentation, a high subset size would probably impair the detection of smaller checks or checks that are tightly spaced. The step size represents the incremental displacement of two adjacent subsets and is equivalent to the density of the measurements. If the subset size depends more on the speckle pattern and optical system characteristics, the step size depends more on the application and the desired spatial resolution. Similar to the subset size, an increase in the subset step decreases the spatial resolution of the strain field map and measured strain (Fig. 8). This is probably because of local peak displacements at small step sizes and the averaging effect at high ones (Wigger et al. 2018). A small subset step is essential to capture individual checks' positions. However, at very low subset steps, e.g. lower than 5 pixels, the precision of the detected check shape was not significantly improved, while the noise and computational cost required were substantially higher.

The precision and resolution of the measurements are impacted by the strain window size, which represents the set difference between adjacent subsets. In our study, the employed DIC algorithm and its settings resulted in a square-shaped strain window equal to the subset step, i.e. 5 pixels, which corresponded to a physical area of approximately  $0.56 \times 0.56$  mm. Consequently, the outputs for check length and width that could be obtained were multiple of this value. While this limitation was deemed to have an insignificant impact on the accuracy of length measurements, it potentially had a more significant effect on the accuracy of width measurements. To account for this specific reason, the measurement of SC disregarded the inclusion of check width and check area measurements, as in the check density index proposed by Burnard et al. (2018). Reducing the physical area corresponding to the strain window size could help alleviate the binning effect on check width measurements. However, achieving this would require careful noise monitoring, a finer DIC pattern and a higher-resolution optical system than those employed in this study.

### 3.4 Method assessment

The DIC method provides advantages over traditional methods, such as visual inspection following a standard

**Fig. 7** Subset size effect on measured strain based on a pretreated EWF specimen's surface captured after 16.5 h exposure time, subset step of 5 pixels for **a**-20, **b**-30, **c**-40 and **d**-50 pixels subset size

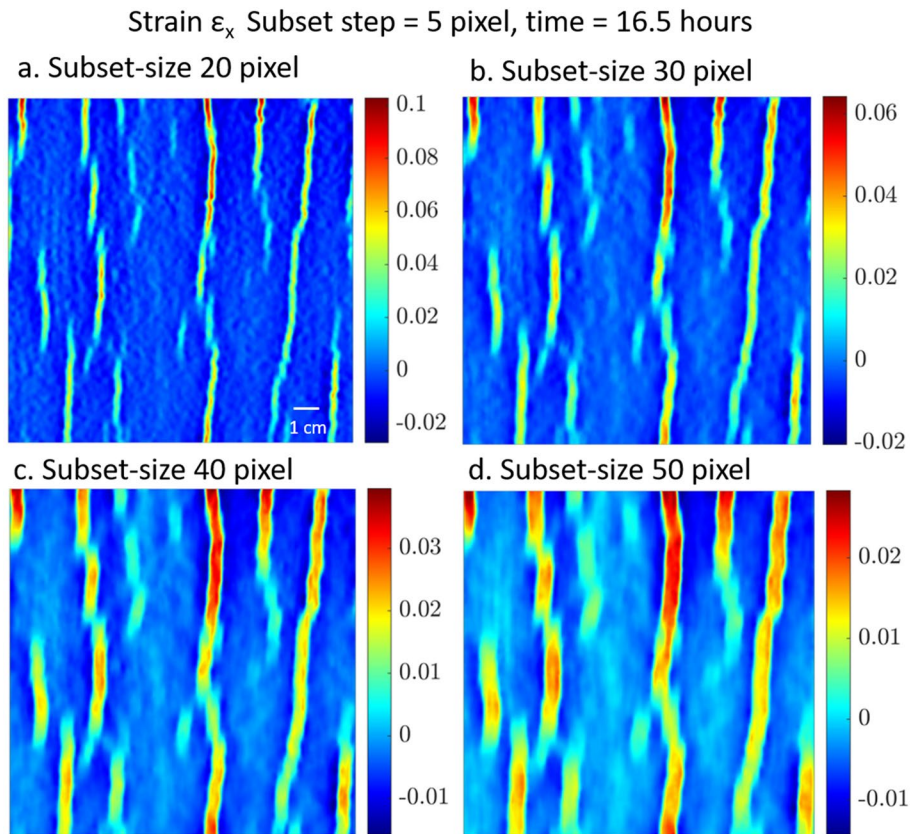
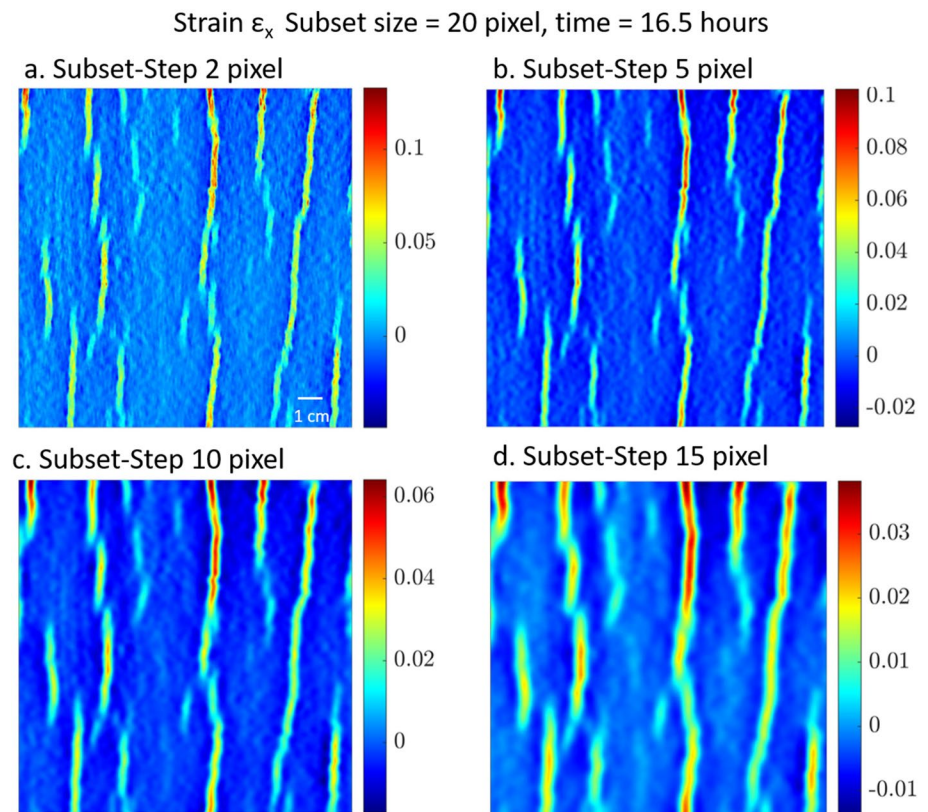


**Fig. 8** Step size effect on measured strain based a pretreated EWF specimen's surface captured after 16.5 h exposure time, subset size 20 pixels for **a**-2, **b**-5, **c**-10 and **d**-15 pixels step size





climate-chamber test, utilising shorter durations, and providing non-contact and automatic measurement. The proposed CI output can be measured with good fidelity despite individual checks being detected as fragmented or joined after the segmentation step. CI could be calculated independently of SL thickness, following the objective of this initial investigation. Further improvements may lie in grouping checks based on their size as a potential qualitative measure and enabling check area measurement with good precision. Another future possible improvement may lie in the segmentation method, such as using a filter processing for the peak gradient detection compared to the global value threshold.

The most important limitations of the method are its destructive nature, specimen preparation resources and measurement bias. Measurement biases were mainly attributed to the DIC settings, optical system and the DIC pattern coating. Some measures to limit bias due to out-of-plane motion in a 2D–DIC system are restricting out-of-plane movement, for example, by adhesion to a base (as in the current study) and increasing lens working distance. Another possible error source of the measured surface strain may be the DIC pattern's coating layer, which could act as a moisture barrier. Future studies should investigate the effects of different DIC pattern systems, e.g. powder coatings, DIC markers, and focus on limiting their impact on surface properties.

## 4 Conclusion

This study illustrates that the DIC method is suitable for SC inspection in SL-based EWF specimens. SC increases significantly with repeated dry-humid environment exposures. Results indicate that the presence of coating reduces SC.

The main findings relate to the testing setup's requirements and the DIC method application and its limitations. Regarding the testing setup, restricting specimen free movement and moisture evaporation limit to the surface were found to facilitate the detection of surface discontinuities related to SC. Regarding DIC post-processing parameters, a low ratio of step size to subset size and a low step size were found beneficial for extended SC detection. A relatively low strain rate threshold was applied to capture small checks.

Further studies would be required to test the method application on a more extended sample size. This would be useful to understand the impact of different structural parameters on SC.

**Acknowledgements** The authors would like to acknowledge Knowledge Foundation for funding the project as part of the industrial research school Prowood+.

**Author contributions** Conceptualisation: VG; methodology: VG; Formal analysis and investigation: VG writing—original draft preparation:

VG; writing—review and editing: VG, JJ, OD; funding acquisition: JJ; resources: JJ; supervision: JJ, OD.

**Funding** Open access funding provided by Linnaeus University. The present work was funded via the Knowledge Foundation fund (KK-Stiftelsen) within the Prowood+ project.

**Availability of data and materials** Data available on request from the authors.

**Code availability** Code available on request from the authors.

## Declarations

**Conflict of interest** On behalf of all authors, the corresponding author states that there is no conflict of interest.

**Open Access** This article is licensed under a Creative Commons Attribution 4.0 International License, which permits use, sharing, adaptation, distribution and reproduction in any medium or format, as long as you give appropriate credit to the original author(s) and the source, provide a link to the Creative Commons licence, and indicate if changes were made. The images or other third party material in this article are included in the article's Creative Commons licence, unless indicated otherwise in a credit line to the material. If material is not included in the article's Creative Commons licence and your intended use is not permitted by statutory regulation or exceeds the permitted use, you will need to obtain permission directly from the copyright holder. To view a copy of this licence, visit <http://creativecommons.org/licenses/by/4.0/>.

## References

- Burnard MD, Muszynski L, Leavengood S, Ganio L (2018) An optical method for rapid examination of check development in decorative plywood panels. *Eur J Wood Prod* 76:1367–1377. <https://doi.org/10.1007/s00107-018-1327-7>
- Cassens D, Leng YL, McCabe G (2003) Face check development in veneered furniture panels. *For Prod J* 53:79–86
- DeVallance DB, Funck JW, Reeb JE (2007) Douglas-fir plywood glue-bond quality as influenced by veneer roughness, lathe checks, and annual ring characteristics. *For Prod J* 57:21–28
- FEP (2021) FEP 2020 Statistics. FEP General Assembly
- Grubfi V, Johansson J (2019) Performance of multi-layered wood flooring elements produced with sliced and sawn lamellas. *Pro Ligno* 15:166–172
- International Digital Image Correlation Society, Jones EMC, Iadicola MA (eds) (2018) A good practices guide for digital image correlation. <https://doi.org/10.32720/idics/gpg.ed1>
- Jonsson R (2005) Studies on the competitiveness of wood: - market segmentation and customer need assessments. PhD Thesis, Växjö University Press
- Kang H-Y, Muszynski L, Milota M (2006) Preliminary tests for optically measuring drying strains and check formation in refractory species. In: Proceedings FPS conference on quality drying for the 21st century, Bellingham., 2006. pp 15–17
- Kang HY, Muszynski L, Milota MR, Kang CW, Matsumura J (2011) Preliminary tests for optically measuring drying strains and check formation in wood. *J Fac Agric Kyushu Univ* 56:313–316
- Leavengood S, Funck JW, Reeb JE (2011) A note on face veneer checking in maple plywood. *Int Wood Prod J* 2:120–123. <https://doi.org/10.1179/2042645311Y.0000000010>

- Legendre P, Legendre L (1998) Numerical ecology, 2nd edn. Elsevier, Amsterdam
- Ludbrook J (2010) Linear regression analysis for comparing two measurers or methods of measurement: But which regression? *Clin Exp Pharmacol Physiol* 37:692–699. <https://doi.org/10.1111/j.1440-1681.2010.05376.x>
- Mallet J, Kalyanasundaram S, Evans PD (2018) Digital image correlation of strains at profiled wood surfaces exposed to wetting and drying. *J Imaging*. <https://doi.org/10.3390/jimaging4020038>
- Pfriem A, Buchelt B (2011) Influence of the slicing technique on mechanical properties of the produced veneer. *Eur J Wood Prod* 69:93–99. <https://doi.org/10.1007/s00107-010-0410-5>
- Wigger T, Lupton C, Tong J (2018) A parametric study of DIC measurement uncertainties on cracked metals. *Strain*. <https://doi.org/10.1111/str.12291>
- Yang J (2020) Augmented lagrangian digital image correlation (2D\_ALDIC). CaltechDATA. <https://doi.org/10.22002/D1.1443>
- Yang J, Bhattacharya K (2019) Augmented lagrangian digital image correlation. *Exp Mech* 59:187–205. <https://doi.org/10.1007/s11340-018-00457-0>

**Publisher's Note** Springer Nature remains neutral with regard to jurisdictional claims in published maps and institutional affiliations.